A&A 596, A88 (2016)
DOI: 10.1051/0004-6361/201628474

Astronomy & Astrophysics

ALMA observations of the Th 28 protostellar disk

A new example of counter-rotation between disk and optical jet

F. Louvet[1], C. Dougados[2,1,3], S. Cabrit[4,3], A. Hales[5,6], C. Pinte[2,1,3], F. Ménard[2,1,3], F. Bacciotti[7], D. Coffey[8], D. Mardones[1], L. Bronfman[1], and F. Gueth[9]

[1] Departamento de Astronomia de Chile, Universidad de Chile, Santiago, Chile
e-mail: flouvet@das.uchile.cl
[2] UMI-FCA, CNRS/INSU, UMI 3386, France
[3] Univ. Grenoble Alpes, CNRS, IPAG, 38000 Grenoble, France
[4] Laboratoire d'Études du Rayonnement et de la Matière en Astrophysique et Atmosphères (LERMA), Observatoire de Paris-Meudon, Paris, France
[5] Atacama Large Millimeter/Submillimeter Array, Joint ALMA Observatory, Alonso de Córdova 3107, Vitacura 763-0355 Santiago, Chile
[6] National Radio Astronomy Observatory, 520 Edgemont Road, Charlottesville, Virginia, 22903-2475, USA
[7] Instituto Nazionale di Astrofisica – Osservatorio Astrofisico di Arcetri, 50125 Firenze, Italy
[8] School of Physics, University College Dublin, Belfield, Dublin 2, Ireland
[9] Institut de Radioastronomie Millimétrique-Grenoble, 38400 Saint-Martin-d'Hères, France

Received 9 March 2016 / Accepted 15 July 2016

ABSTRACT

Aims. Recently, differences in Doppler shifts across the base of four close classical T Tauri star jets have been detected with the HST in optical and near-ultraviolet (NUV) emission lines, and these Doppler shifts were interpreted as rotation signatures under the assumption of steady state flow. To support this interpretation, it is necessary that the underlying disks rotate in the same sense. Agreement between disk rotation and jet rotation determined from optical lines has been verified in two cases and rejected in one case. Meanwhile, the near-ultraviolet lines, which may trace faster and more collimated inner spines of the jet than optical lines, either agree or show no clear indication. We propose to perform this test on the fourth system, Th 28.

Methods. We present ALMA high angular resolution Band 7 continuum, ^{12}CO(3−2) and ^{13}CO(2−1) observations of the circumstellar disk around the T Tauri star Th 28.

Results. The sub-arcsecond angular resolution ($0.46'' \times 0.37''$) and high sensitivity reached enable us to detect, in CO and continuum, clear signatures of a disk in Keplerian rotation around Th 28. The ^{12}CO emission is clearly resolved, allowing us to derive estimates of disk position angle and inclination. The large velocity separation of the peaks in ^{12}CO, combined with the resolved extent of the emission, indicate a central stellar mass in the range 1−2 $M_{\odot}$. The rotation sense of the disk is well detected in both ^{13}CO and ^{12}CO emission lines, and this direction is opposite to that implied by the transverse Doppler shifts measured in the optical lines of the jet.

Conclusions. The Th 28 system is now the second system, among the four investigated so far, where counter-rotation between the disk and the optical jet is detected. These findings imply either that optical transverse velocity gradients detected with HST do not trace jet rotation or that modeling the flow with the steady assumption is not valid. In both cases jet rotation studies that rely solely on optical lines are not suitable to derive the launching radius of the jet.

Key words. stars: individual: Th 28 – ISM: jets and outflows – techniques: interferometric – submillimeter: ISM – stars: formation – circumstellar matter

1. Introduction

The interplay between accretion and ejection of matter is believed to be a crucial element in the formation of stars. Yet, the exact link between jets and accretion disks is still a critical issue in contemporary astrophysics (Ray et al. 2007). The most attractive possibility is a fundamental connection via angular momentum transfer from disk to jet by means of magnetocentrifugal forces, so that circumstellar material may continue to accrete onto the central object (e.g., Blandford & Payne 1982). Exactly where this transfer occurs and how it impacts the disk physics is, however, still hotly debated (Ferreira et al. 2006; Pudritz et al. 2007; Shang et al. 2007; Romanova et al. 2009; Cabrit 2009). Owing to their low extinction and their proximity (≈150 pc), accreting classical T Tauri stars (hereafter CTTSs) offer a unique laboratory to elucidate the connection between accretion and ejection.

A recent major breakthrough was the detection with the STIS instrument mounted on the HST of transverse Doppler shifts of 5−30 km s^{-1} in optical and near-ultraviolet (hereafter NUV) emission lines on scales of 50 au across the base of four close CTTS jets (Bacciotti et al. 2002; Woitas et al. 2005; Coffey et al. 2004, 2007). If these shifts are due to jet rotation in a steady state outflow, they would imply that jets are magnetically launched from the disk surface at relatively small-scale radii of 0.1−1.6 au, thus solving the long-standing problem of the jet origin in CTTS

Table 1. Main observational parameters.

Parameter	^{12}CO	^{13}CO	Continuum
Frequency	345.8 GHz	330.6 GHz	332.0 GHz[a]
Bandwidth	469 MHz	469 MHz	2 GHz
Native channel width	122 kHz	122 kHz	15625 kHz
Primary beam	18.2″	19.0″	18.9″
Synthesized beam	0.″46 × 0.″37	0.″49 × 0.″39	0.″50 × 0.″39
Beam position angle	87.5°	87.8°	90.0°
1σ rms[b]	∼21 mJy/beam km s^{-1}	∼23 mJy/beam km s^{-1}	∼0.078 mJy/beam

Notes. [(a)] The mean frequency was calculated assuming a $S(\nu) \propto \nu^{-3}$ emission spectrum which accurately describes the ISM SED slope in the 2 GHz spectral window. [(b)] The rms presented here report 1σ rms of the integrated maps shown in Fig. 1.

(Bacciotti et al. 2002; Anderson et al. 2003; Coffey et al. 2004; Woitas et al. 2005). However, effects other than rotation (e.g., precession; see Cerqueira et al. 2006) could cause transverse Doppler shifts similar to those detected in T Tauri jets. It is crucial that the underlying disks rotate in the same sense as the jet to support the jet rotation interpretation. This comparison was conducted in three of the four systems mentioned above (CW Tau, DG Tau, and RW Aur), plus in RY Tau. In RY Tau, the study was inconclusive as no systematic Doppler shifts were found in the jet; see Coffey et al. (2015). The sense of rotation of the jets of CW Tau and DG Tau (Coffey et al. 2007), traced by optical lines, coincides with the sense of rotation of their disks (Testi et al. 2002; Cabrit, priv. comm., respectively). The jet rotation sense traced in near ultra-violet (NUV) emission lines at higher flow velocities is coherent for DG Tau, but these emission lines are below the detection threshold for CW Tau (Coffey et al. 2007). In RW Aur, the optical jet and disk rotations appear opposite (see Coffey et al. 2004; Cabrit et al. 2006). Here, jet rotation traced in the NUV was found to be compatible with the disk rotation sense (i.e., opposite to the optical jet rotation), but could only be measured in one lobe and at one of the two epochs (spaced by six months; see Coffey et al. 2012); because of its complexity and variability the authors declared RW Aur as unsuitable for jet rotation studies. We present the confrontation of jet and disk rotation senses for the fourth system, Th 28.

The T Tauri star ThA 15−28 (hereafter Th 28; The 1962), also known as Sz 102 (Schwartz 1977) or Krautter's star, is a young member of the Lupus 3 association. Although uncertain, as the photospheric spectrum is veiled, a spectral type G8 to K2 was quoted for the central object of Th 28 (Graham & Heyer 1988; Hughes et al. 1994; Mortier et al. 2011). Even for a K star, the stellar emission from Th 28 is significantly underluminous: 0.03 $L_\odot$ (Mortier et al. 2011), which suggests that the disk is observed close to edge-on and obscures the central star. The derived disk luminosity, inferred from the spectral energy distribution (SED) integrated excess above the stellar photosphere, is ∼0.13 $L_\odot$ (Mortier et al. 2011; Merín et al. 2008). We adopt the recent value of $d = 185^{+11}_{-10}$ pc derived by Galli et al. (2013) for the Lupus 3 cloud, with an improved convergent point search method, for the distance to the source.

Th 28 drives a bright and striking bipolar jet whose axis lies at PA = 98° (Krautter 1986; Graham & Heyer 1988). The large proper motions derived for the distant knots are compatible with a close to edge-on geometry (e.g., Comerón & Fernández 2010). Th 28 is considered one of the best case for jet rotation detection in the HST sample, as transverse velocity gradients are well detected in both lobes of its optical atomic jet and are consistent in different optical lines (Coffey et al. 2004). In optical, the jet rotation sense is therefore well determined with a clockwise direction looking down the blueshifted jet lobe toward the source. The situation for NUV lines were inconclusive (Coffey et al. 2007). Only one measurement on the receding jet, that is, however, consistent with the sense of rotation derived in optical, exceeded the incertitude level.

In this paper, we report ALMA band 7 CO and continuum observations at 0.4″−0.5″ angular resolution of the Th 28 system, aimed to detect the disk and determine its sense of rotation. We detail our observations and data reduction in Sect. 2, and demonstrate that the CO and continuum emissions clearly trace a disk in Keplerian rotation around Th 28 in Sect. 3. Section 4 offers a detailed analysis of the disk properties. In Sect. 5 we discuss the implications for jet launching models and central source properties. We summarize our conclusions in Sect. 6.

2. Observations and data reduction

The characteristics of our lines and continuum observations are detailed below. The resulting beam sizes and sensitivities are summarized in Table 1.

The ^{12}CO($J = 3 \rightarrow 2$) and ^{13}CO($J = 3 \rightarrow 2$) emission lines plus the continuum emission of Th 28 were observed using ALMA Band 7 (275−373 GHz). The observations were performed on April 28 2014 in two tracks of ∼40 min each during the ALMA cycle 1 campaign. The Band 7 data contained two spectral windows of 468.75 MHz bandwidth each (3840 channels) that were tuned at 345.818 GHz and 330.609 GHz. This allowed us to simultaneously cover the ^{12}CO($J = 3 \rightarrow 2$) and ^{13}CO($J = 3 \rightarrow 2$) at 345.796 GHz and 330.588 GHz, respectively. A third spectral window of 2 GHz bandwidth in 128 channels centered at 332.014 GHz was dedicated to the detection of the continuum emission from the Th 28 dust disk. The phase center of the observations was taken to be the position of Th 28 as seen with HST: $\alpha(J2000) = 16^{\rm h}08^{\rm m}29\overset{\rm s}{.}72$ and $\delta(J2000) = -39°03'11\overset{''}{.}01$. The data were taken using the cycle 1 semi-extended configuration of ALMA with baselines ranging from 20 m to 480 m.

The data were reduced using the common astronomy software application (hereafter CASA; see McMullin et al. 2006). We performed an initial correction for rapid atmospheric variations at each antenna using water vapor radiometer data and corrected for the time and frequency dependence of the system temperatures. Bandpass calibration was performed on the quasars J1733-1304 and J1517-2422. The primary flux calibration was made using Titan and J1517-2422. Quasar J1534-3526 was used in both observations to calibrate the time variation of the complex gains. Based on the dispersion between the fluxes derived for the phase calibrator in each observing session (using the two different amplitude calibrator), we estimate the absolute

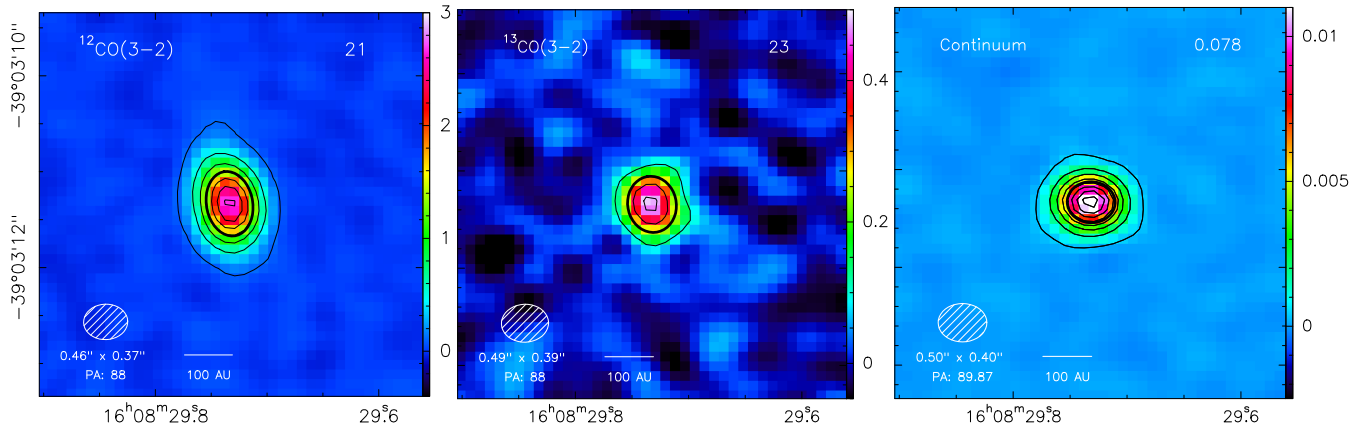

Fig. 1. *Left*: moment zero of the ^{12}CO(3−2) integrated from −15 to 20 km s^{-1}. Contours start at 5σ with 20σ steps. *Middle*: moment zero of the ^{13}CO(3−2) integrated from −15 to 20 km s^{-1}. Contours start at 5σ with 5σ steps. *Right*: continuum map. Contours start at 5σ with 20σ steps. Noise level at 1σ is indicated in the upper right corner of each panel; the unit is mJy/beam km s^{-1} in the two left panels and mJy/beam in the right panel. The black ellipses on the three panels represent the FWHM intensity contours. White hatched ellipses represent the clean beam FWHM.

flux calibration to be accurate within ∼10%. Owing to residual inconsistency in the phase calibration between the two tracks, we used the continuum spectral window of one track to further phase calibrate all spectral windows. Imaging was carried out using the CLEAN algorithm of CASA. We used the Briggs weighting with a robust parameter of 0.5[1]. The channel spacing of 0.122 MHz resulted in a maximum spectral resolution of ∼0.11 km s^{-1} that we degraded down to 0.4 km s^{-1} to detect weak ^{12}CO and ^{13}CO emission. The resulting root mean square (rms) noise level is of 4 mJy/beam per 0.4 km s^{-1} channel in ^{12}CO(3−2) and ^{13}CO(3−2). The continuum displays a rms noise of 0.08 mJy/beam over its 2 GHz bandwidth. Panels a, b, and c in Fig. 1 (left, middle, and right) show the ^{12}CO(3−2), ^{13}CO(3−2), and continuum, respectively, which will be described in Sect 3.

3. Results

3.1. CO emissions probing a disk in Keplerian rotation

Left panels of Fig. 1 show CO emission maps integrated over the velocity interval [−15 km s^{-1}, 20 km s^{-1}]. Both CO lines are clearly detected and centered at the source position with an integrated flux of 5.1 Jy km s^{-1} in ^{12}CO and 0.60 Jy km s^{-1} in ^{13}CO. The top panel of Fig. 2 shows the integrated spectra of the ^{12}CO(3–2) and of the ^{13}CO(3–2) inside the area defined by the 5σ contours of Fig. 1 (left) and Fig. 1 (middle), respectively. The morphology and kinematics of the CO emission show clear signatures of a protoplanetary disk in Keplerian rotation:

(a) The emission is compact (<200 au) and elongated in ^{12}CO.
(b) The elongation is perpendicular to the atomic jet position angle (PA).
(c) The CO lines show the double-peaked shape characteristic of a disk in Keplerian rotation.
(d) The position-velocity diagram along the PA of the disk is also compatible with a disk in Keplerian rotation.

We detail each of these items below.

(a) Compact and elongated CO emission: the ^{12}CO emission shows an elliptical shape with a main axis close to the north-south direction, roughly perpendicular to the main axis of the beam. It is therefore clearly resolved in the north-south direction. Indeed, the emitting area with fluxes above half maximum emission is an ellipse of 0.68″ × 0.48″ at PA ≈ 10° (black ellipse in Fig. 1, left) while the beam is 0.46″ × 0.37″ at PA ≈ 88°. The ^{13}CO displays a more compact emission than the ^{12}CO. The area of half maximum emission corresponds to an ellipse of 0.58″ × 0.50″ at PA ≈ 10° (see black ellipse in Fig. 1, middle). When compared to the beam size, 0.49″ × 0.39″ at PA ≈ 88°, the ^{13}CO appears only marginally resolved in the north-south direction. The compact scale of the emission argues against an origin in an infalling envelope. The CO emission therefore most likely traces the accretion disk around Th 28.

(b) CO emission perpendicular to the PA of the atomic jet: to derive the intrinsic size and geometry of the CO emission, we performed 2D-Gaussian fits directly in the *uv* plane with the UV-FIT procedure of GILDAS[2]. The result of these fits are reported in Table 2. The 2D-Gaussian fits have FWHM of 0.82 ± 0.01″ × 0.24 ± 0.01″ at a PA = 7.3 ± 0.4° in ^{12}CO and 0.66 ± 0.03″ × 0.19 ± 0.09″ at PA = 7.6 ± 3.7° in ^{13}CO.
The PA of the long axis of the CO emissions (see (a) and (b)) are therefore perpendicular, within the uncertainties, to the PA of the optical blueshifted jet (98°).

(c) Double-peaked profile of the CO lines: the integrated CO line profiles are double peaked with symmetric wings (see Fig. 2, top), exhibiting a strong resemblance to the typical profile shape of rotating Keplerian disks in CTTS (Duvert et al. 2000; Guilloteau & Dutrey 1994). The ^{12}CO and ^{13}CO show peak fluxes of ∼0.45 Jy and 0.04 Jy, respectively. The apparent separations of the two velocity peaks toward Th 28 is larger in ^{13}CO than in ^{12}CO: Δv = 8.7 ± 0.1 km s^{-1} and 7.1 ± 0.3 km s^{-1}, respectively. Such a behavior is expected for a Keplerian disk, since the intensity peaks roughly correspond to the outer radius of the disk, which should be larger in the more optically thick ^{12}CO(2−1) line.

(d) The position-velocity (PV) diagram of the ^{12}CO emission line along the PA = 7.3° of the disk is shown in Fig. 3. It further confirms the hypothesis of a disk in rotation with a quasi-perfect point symmetry both in position and velocity. Such a pattern is indeed indicative of a globally axisymmetric rotating structure around Th 28. We have

[1] Therefore giving slightly more weight to the longest baselines than with natural weighting.

[2] See the following webpage for details: IRAM.

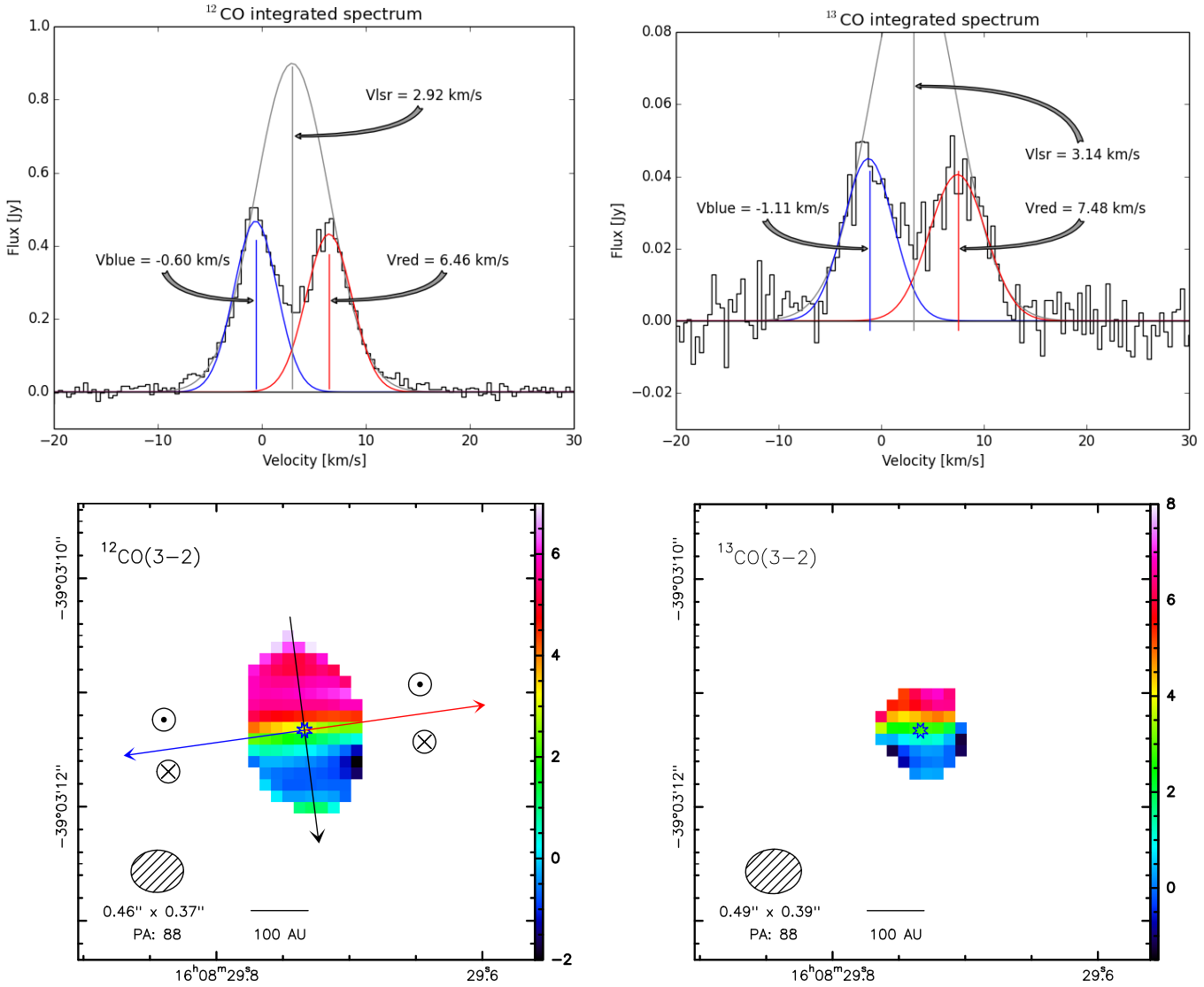

Fig. 2. *Top left*: integrated spectra of the ^{12}CO(3−2) emission line. *Top right*: integrated spectra of the ^{13}CO(3−2) emission line. The integration surfaces correspond to areas where emission is above 5σ on the corresponding integrated maps presented in Fig. 1. *Bottom left*: first moment of the ^{12}CO(3−2) emission line. The black arrow indicates the PA of the disk as seen in ^{12}CO. The latter is used to build the PV diagram shown in Fig. 3. The red and blue arrows represent the jet axis of Th 28, while the line-of-sight vectors represent their rotation sense in optical tracers derived by Coffey et al. (2004). *Bottom right*: first moment of the ^{13}CO(3−2) emission line. In these two first-moment maps, a clear velocity gradient due to the rotation of the circumstellar disk of Th 28 is seen.

superimposed Keplerian curves for stellar central masses $M_\star$ = 1, 2, and 3 $M_\odot$ (see Sect. 5.2 for a more detailed analysis), assuming the disk has an inclination of 73 degrees.

With the supporting evidence presented above, we claim to observe a protoplanetary disk in Keplerian rotation around Th 28.

3.2. Continuum emission of the disk

Figure 1 (right) shows the 0.9 mm continuum emission of Th 28, centrally peaked at the position of the source. With a signal-to-noise (S/N) ratio of ∼150, we report the unambiguous detection of continuum emission in the circumstellar disk of Th 28. The comparison of the beam (0.50″ × 0.40″ with PA of 88.8°) to the emission area with fluxes above half of the peak flux (0.50″ × 0.41″ with PA of 88.0°) indicates unresolved continuum emission from Th 28 at 0.90 mm. The mm-dust emission is therefore compact, in accordance with an emission originating from a disk.

As for the line results (see Sect. 3.1), to free ourselves of deconvolution uncertainties, we performed a fit of the disk parameters in the *uv* plane. Keeping in mind that the continuum appears unresolved in the image plane, it reveals a disk of ∼0.26″ × 0.10″ at PA = 15 ± 4° (see Table 2), which is roughly compatible with those derived in ^{12}CO & ^{13}CO.

Mass of the disk. If we assume optically thin emission from dust grains at T = 20 K, a dust opacity coefficient k_ν = 0.1 cm^2 g^{-1} × (ν/1000 GHz)$^\beta$ (very similar to that advocated by Hildebrand 1983, including a gas to dust ratio of 100 by mass) with β ∼ 0.5 (Beckwith & Sargent 1991), our total flux density of 13.3 mJy implies a total mass of ∼8.5 × 10^{-4} $M_\odot$ at the distance of 185 pc of Th 28. This circumstellar disk mass is relatively low but is not inconsistent with known CTTS disk masses (4 × 10^{-3} $M_\odot$ with a 0.72 dex standard deviation; Andrews & Williams 2005). Also, this value is highly sensitive to the assumptions made on the parameters listed above. For

Table 2. Fit to the observable features.

Parameter	Flux[a]	Elliptical Gaussian fit in the *uv* plane[b]				V_{lsr}[c]	Peak separation
		Major axis	Minor axis	PA	Inclination	–	Δv
	Jy	[″]	[″]	[°]	[°]	[km s^{-1}]	[km s^{-1}]
^{12}CO	5.10	0.82 ± 0.01	0.24 ± 0.01	7.3 ± 0.4	73 ± 1	2.92 ± 0.05	7.1 ± 0.1
^{13}CO	0.60	0.67 ± 0.03	0.19 ± 0.09	7.6 ± 3.7	73 ± 9	3.14 ± 0.10	8.7 ± 0.3
Continuum	13.3×10^{-3}	0.26 ± 0.01	0.09 ± 0.04	15 ± 4	69 ± 11	–	–

Notes. [(a)] Integrated fluxes inside the area defined by a 5σ contour. The emission lines are integrated in the −15 to 20 km s^{-1} range. [(b)] The fits in the *uv* plane are centered at the following coordinates, $\alpha(J2000) = 16^h08^m29\overset{s}{.}73$ and $\delta(J2000) = -39°03'11\overset{''}{.}33$. [(c)] The central velocities are determined from the fit of a single Gaussian to the wings of the spectra (see Fig. 2, top)

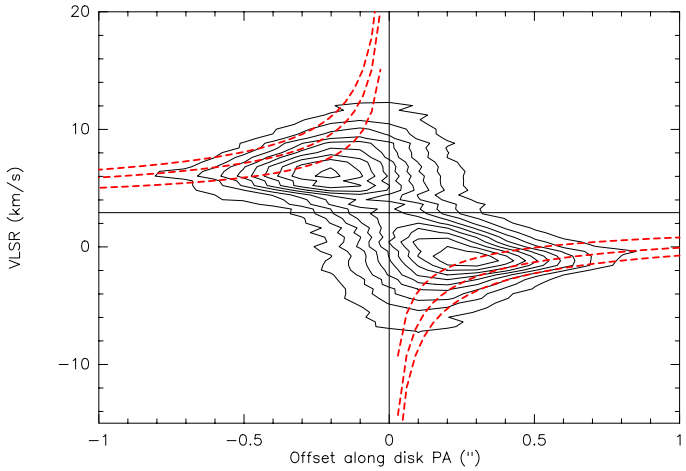

Fig. 3. PV diagram of the ^{12}CO emission along the disk PA (see black arrow in Fig. 2, bottom left). Contour star at 32 mJy/beam with 32 mJy/beam steps. The plot is superimposed with expected Keplerian motions in a disk inclined by 80° for a central object of 1, 2, and 3 $M_\odot$ (internal, central, and external curves respectively).

instance a variation of −20% (resp. +20%) of the dust temperature implies an augmentation (resp. diminution) of the disk total mass to $1.2 \times 10^{-3}\ M_\odot$ (resp. $6.6 \times 10^{-4}\ M_\odot$), while varying the opacity index β by minus or plus 20% changes the total disk mass to $7.6 \times 10^{-4}\ M_\odot$ and $9.4 \times 10^{-4}\ M_\odot$, respectively.

4. Analysis

4.1. V_{lsr} of the source

To determine the V_{lsr} of Th 28, we fitted a single Gaussian component to the high-velocity wings of the ^{12}CO and ^{13}CO profiles (see top of Fig. 2 and Table 2). We derived a central velocity of $V_{lsr} \approx 2.92$ km s^{-1} in ^{12}CO and $V_{lsr} \approx 3.14$ km s^{-1} in ^{13}CO. In the following, we adopt a $V_{lsr} = 3 \pm 0.1$ km s^{-1} for Th 28. This value is compatible with the range of V_{lsr} observed toward the Lupus 3 cloud (James et al. 2006).

4.2. Disk inclination

The CO emission aspect ratio derived from the 2D-Gaussian fits in the *uv* plane provides estimates of the inclination to the line of sight of 73 ± 1° and 73 ± 9° from the ^{12}CO and ^{13}CO emission lines, respectively (see Table 2). This inclination is comparable but somewhat lower than the inclination of 82.3 ± 2° for the optical jet determined from the proper motions of distant knots (see Appendix A). However, the CO emission may be underestimating the true disk inclination. Indeed, CO emissions are expected to arise above the disk plane at typical altitudes of 2−3 disk scale heights (Dartois et al. 2003). For a close to edge-on geometry, the apparent ellipse in the plane of the sky has a larger semiminor axis than a flat disk, mimicking a less inclined flat disk.

4.3. Disk rotation sense

The lower panels of Fig. 2 show the first moment map of the ^{12}CO(3−2) and ^{13}CO(3−2) emission lines. A velocity gradient along the PA of the disk is striking from those plots. They reveal that the northeastern part of the disk is redshifted, while the southwestern part is blueshifted. We therefore report unambiguous detection of the sense of rotation of the Th 28 disk. The derived sense of rotation is opposite that derived for the optical jet with the HST (see Fig. 2). We discuss the implications of this result for jet launching models in the following section.

4.4. ^{12}CO versus ^{13}CO

To derive the overall flux ratio of the ^{13}CO emission line with respect to the ^{12}CO emission line, we integrated both lines (i) in the velocity range −15 km s^{-1} to 20 km s^{-1} and (ii) over the area where the ^{13}CO displays fluxes above 5σ (see Fig. 1 − Middle). In so doing, we achieve integrated fluxes of ∼3.75 Jy km s^{-1} and ∼0.60 Jy km s^{-1} for the ^{12}CO and ^{13}CO, respectively. The integrated flux ratio, S(^{13}CO)/S(^{12}CO), is therefore of ∼0.16. The discrepancy between the integrated flux ratio (0.16) and the fractional abundance of CO isotopes ([^{13}CO]/[^{12}CO] ∼ 0.017 in the ISM) implies the ^{12}CO to be optically thick. Nevertheless, an optically thick ^{12}CO line profile supplies a valuable indication on the temperature profile in the disk (Beckwith & Sargent 1993, hereafter BS93); see Sect. 4.5.

4.5. Temperature profile (T(K) versus radius) in the disk

Since the ^{12}CO emission line is optically thick (see above), its spectrum is a direct probe of the temperature as a function of radius. Following the analysis developed by BS93, if the temperature profile follows a power law in radius (r), as $T \propto r^{-q}$, the flux density is roughly proportional to v_{obs}^{3q-5} in the high-velocity wings. Performing the fit of the flux density on the high-velocity blue wing [−8.0 km s^{-1}; −2.4 km s^{-1}] of the ^{12}CO emission line, we find an index $q = 0.8 \pm 0.2$. Under these assumptions, the temperature profile of Th 28 is steeper than the typical values derived in CTTS disks (0.5−0.75; see Isella et al. 2009; Beckwith & Sargent 1991).

5. Discussion

Our ALMA observations of Th 28 reveal, for the first time, the millimeter CO and continuum emission from its accretion disk. We first discuss the implications brought by these observations for jet rotation studies. We then briefly discuss additional first order constraints on the Th 28 system.

5.1. Implications for jet rotation studies

Our high S/N ratio and well-behaved ALMA CO observations unambiguously establish that the Th 28 disk rotates in a sense opposite to that derived with the HST for both lobes of the Th 28 atomic optical jet by Coffey et al. (2004). Now, consistency between disk and jet rotation has been investigated in five systems. One was not informative, since the jet rotation sense could not be detected (RY Tau). Two of them (DG Tau, CW Tau) show consistent disk and optical jet rotation sense, while the two others (RW Aur and now Th 28) show inconsistent rotation sense. However, RW Aur-A is peculiar since its star shows periodic radial velocity variations possibly signaling a close companion (Petrov et al. 2001), which might confuse its jet dynamics, for example, through jet precession/wiggling or shock asymmetries (Cerqueira et al. 2006). On the contrary, the Th 28 jet was one of the best cases of jet rotation detection, with different optical lines and both lobes of the jet giving similar transverse velocity gradients. So, the discrepancy observed in that most favorable case between jet and disk rotation suggests broader implications for optical jet rotation studies. We discuss below three possible explanations for the observed discrepancy:

1) The disk rotation is probed on radial distances $r \geq 20$ au from the source, while the jet is expected to originate from much smaller disk radii, $r < 5$ au (Ray et al. 2007). One could imagine either a true change of rotation sense in the inner disk regions or a warp between the inner and outer disk that could induce an artificial change of rotation sense in the outer disk due to projection effects. Although we cannot fully exclude these possibilities, they seem unlikely as both the inclination and the PA of the outer CO disk axis agree well with that of the atomic jet, indicating no significant change of disk geometry between au to tens of au scales. In addition, the high inclination of the outer disk rotation axis means that line-of-sight velocities are very close to the underlying disk rotation velocities and that projection effects should be minimized. Moreover, the disk of Th 28 does not show any evidence of perturbation in its PV diagram at high velocities that could betray such behavior.
2) The observed transverse velocity gradients in jets do trace rotation but in a nonstationary part of the flow. Indeed, shocks and/or nonstationary ejection may significantly alter the apparent rotation of the flow, either amplifying it (Fendt et al. 2011) or even reversing it (Sauty et al. 2012) owing to the exchange of angular momentum between the flow and the magnetic field. Also, Staff et al. (2015) recently presented 3D magnetohydrodynamic simulations of disk winds where the less opened magnetic field configuration results in a wide, two-component jet. They show that kink mode creates a narrow corkscrew-like jet with regions in which jet rotation at ±2 au from its axis is opposite to the disk. However such counter-rotating jet signatures would remain unresolved at the current achievable angular resolution of 0.1″ (=14 au) with the HST in the optical domain.
3) Optical transverse velocity gradients in jets do not trace rotation in the jet body but rather a departure from axisymmetry. Indeed, high angular resolution observations show evidence of small-scale jet axis wiggling and/or asymmetric shock fronts (see, e.g., White et al. 2014; Coffey et al. 2015). White et al. (2014) recently demonstrated in the DG Tau case that spurious rotation signatures on the same magnitude as those observed in the optical can be mimicked if the jet axis wiggling is not properly taken into account. Moreover, transverse velocity gradients traced by optical emission lines probe an intermediate velocity component (IVC) of the flow, the nature of which is still unclear. White et al. (2014) proposed that the IVC in DG Tau traces a dragged mixing layer between a fast inner jet and an outer slower wind. Therefore, transverse gradients detected in the NUV domain, which probe a faster and more collimated component of the flow, may trace jet rotation more reliably. The NUV velocity gradients detected in two sources so far (DG Tau and RW Aur) appear to rotate in the same sense as their underlying disks. However, RW Aur shows a time-variable behavior that renders it unsuitable for jet rotation studies. In the case of Th 28 no sense of rotation could be reliably determined in the NUV. Difficulties were encountered in this plane-of-sky jet because of a large, low-velocity absorption feature that closely coincides with the jet radial velocity. Further studies are clearly needed to establish whether observed NUV velocity gradients do indeed trace jet rotation.

In any case, the implications are that the velocity gradients derived from optical lines in T Tauri jets cannot be used to infer jet launching radius using the method proposed by Bacciotti et al. (2002), Anderson et al. (2003), Ferreira et al. (2006). Indeed, application of this method requires that the flow is both stationary and axisymmetric. Both assumptions seem inconsistent with the discrepancy found between the optical jet and disk rotation sense in Th 28.

5.2. Implications for the nature of Th 28

Comerón & Fernández (2010) derived a central stellar mass of 0.6−0.9 $M_\odot$ from the maximum velocity of 450 km s^{-1} observed in the redshifted wings of the Hα emission line profile, assuming that this velocity traces the free-fall velocity of infalling gas at the base of the accretion columns. In the following, we argue that the combination of the spatial extension and peak velocity separation observed in ^{12}CO indicates a stellar mass more in the range 1−2 $M_\odot$.

An accurate derivation of the central stellar mass would require a detailed disk modeling, with radiative transfer effects properly taken into account, and fits of the spectral energy distribution. Such a detailed analysis goes beyond the scope of the present paper. Instead, we propose a simple derivation of the central stellar mass standing on the ^{12}CO emission line. To meaningfully constrain the central stellar mass from the position-velocity diagram, it is critical to take projection and beam convolution effects into account. To do so, we build a simple geometrical model of an optically thick flat disk with a radial power law temperature distribution of index q and we convolve this model with the effective ALMA beam of the ^{12}CO observations. We fix the disk inclination to $i = 80°$ and the power law index q of the temperature profile to $q = 0.8$, which is most compatible with the shape of the wings in the ^{12}CO profile (see Sect. 4.5). In order to reproduce the observed ^{12}CO brightness profile along the disk major axis, a disk outer radius of $R_{\rm out} = 0.5''$ is required, corresponding to 92.5 au at the adopted distance of $d = 185$ pc for Th 28. The observed velocity separation between the peaks is

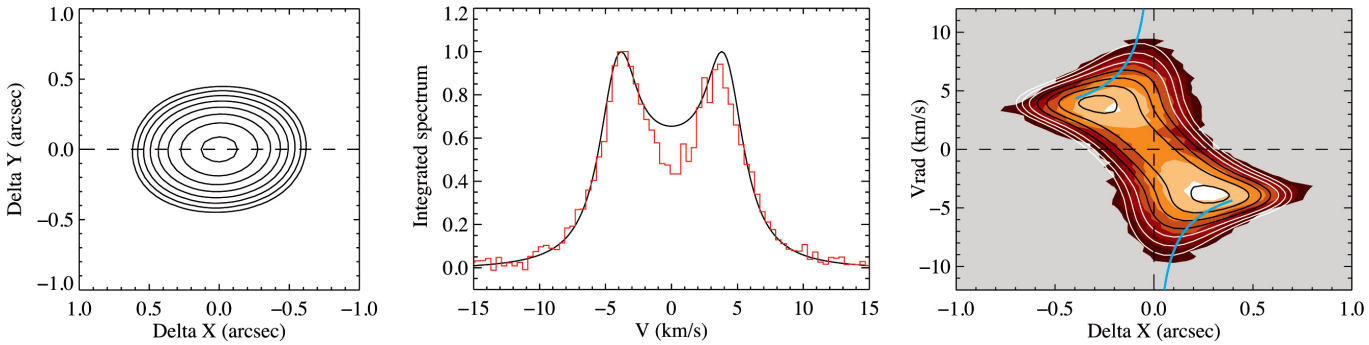

Fig. 4. Predictions of the ^{12}CO emission for flat, optically thick disks viewed at 80° inclination. The model corresponds to a solution with $R_{\rm out}$ = 92.5 au, $M_\star$ = 1.6 $M_\odot$. The model was convolved with a beam of 0.46″ by 0.37″ with a PA = 88°. *Left panel*: predicted ^{12}CO integrated intensity map; *middle panel*: ^{12}CO integrated spectra (data en red and model in black); *right panel*: predicted position-velocity diagram along the disk PA (black and white contours) overlaid on observations (background color map). The blue curve shows the theoretical projected Keplerian velocity profile. In all maps, contours start at 90% of the peak and decrease by $\sqrt{2}$.

then best fitted with a stellar mass of 1.6 $M_\odot$. The model described above depends on the index of the temperature profile, q, whose value is uncertain by 25% (see Sect. 4.5). Spreading this uncertainty in the model, we derive an uncertainty on the mass of the central star of ±0.2 $M_\odot$. Moreover, a central stellar mass in the range 1−2 $M_\odot$ appears more compatible with a spectral type of early K as quoted in the literature for this object. Using the pre-main-sequence tracks of Siess et al. (2000), a spectral type of K2 ($T_{\rm eff}$ = 4900−5000 K) corresponds to $M_{\rm star} \geq 2\,M_\odot$ for ages less than 3.5 Myr.

Concerning the low luminosity of the central object, our best fit to the CO emission profiles gives $V_{\rm lsr}$ = 3 ± 0.1 km s^{-1}, which is consistent with the range of values observed in the Lupus 3 cloud (James et al. 2006). It is then unlikely that the low luminosity of the central Th 28 star could be related to a larger distance. One would expect before extinction a ∼1.9 $L_\odot$ luminosity from a 1.5 $M_\odot$ protostar of age ≤3.5 Myr (Siess et al. 2000)[3]. Therefore an extinction of 4.5 mag would be sufficient to attenuate the star down to the luminosity observed for Th 28 (0.03 $L_\odot$, see Mortier et al. 2011). Such an extinction appears easily achievable from a close to edge-on system and our ALMA observations confirm a large inclination to the line of sight ($i \geq 73°$). This is also consistent with the fast proper motion of the jet knots at the distance of Lupus 3 when compared to their radial velocities (see Sect. 4.2).

6. Conclusions

We have observed the T Tauri star Th 28 during the ALMA-cycle 1 campaign in Band 7 (275−373 GHz). We detected ^{12}CO(J = 3 → 2), ^{13}CO(J = 3 → 2) and continuum signatures of a Keplerian accretion disk around Th 28.

- The ^{12}CO emission is clearly resolved and elongated along PA = 7.3°. The morphology of the disk seen in CO matches very well the morphology derived for the large-scale atomic jet. The PA of the disk is perpendicular to that of the jet, and both inclinations are comparable.
- The ^{12}CO shows kinematics that are consistent with a disk in Keplerian rotation. Indeed its double-peak integrated profile, plus its PV diagram along the PA of the disk, are characteristic of Keplerian rotation.
- We derive a $V_{\rm lsr}$ = 3 ± 0.1 km s^{-1} for the central source in agreement with the range of values observed in the Lupus 3 cloud.
- We constrain the power law index, q, of the temperature distribution to $q \simeq 0.8$ and the $R_{\rm out}$ to ≃92.5 au.
- The combination of large $R_{\rm out}$ and peak velocity separation in ^{12}CO of Δv = 7 km s^{-1} is best reproduced with a central stellar mass of 1.4−1.8 $M_\odot$. This is also consistent with early K spectral type estimates for this source.
- The rotation sense of the disk is well detected with our ALMA CO observations and this direction is opposite that of the transverse velocity shifts previously detected with HST in the optical jet. This discrepancy in rotation senses implies that velocity gradients measured in optical lines cannot be used to infer launching radii. The NUV domain, which probes a faster and more collimated inner part of the jet, is likely more reliable to measure jet rotation from Doppler gradients.

Acknowledgements. F.L. acknowledges support from the Joint Committee ESO government of Chile. F.L. thanks Simón Casassus (Universidad de Chile) for his careful reading of the paper and numerous comments that led to extensive discussions among the authors. L.B. acknowledges support by CONICYT Grant PFB-06. This paper makes use of the following ALMA data: ADS/JAO.ALMA#2012.1.00857.S. ALMA is a partnership of ESO (representing its member states), NSF (USA) and NINS (Japan), together with NRC (Canada), NSC and ASIAA (Taiwan), and KASI (Republic of Korea), in cooperation with the Republic of Chile. The Joint ALMA Observatory is operated by ESO, AUI/NRAO and NAOJ. The National Radio Astronomy Observatory is a facility of the National Science Foundation operated under cooperative agreement by Associated Universities, Inc.

References

Anderson, J. M., Li, Z.-Y., Krasnopolsky, R., & Blandford, R. D. 2003, ApJ, 590, L107
Andrews, S. M., & Williams, J. P. 2005, ApJ, 631, 1134
Bacciotti, F., Ray, T. P., Mundt, R., Eislöffel, J., & Solf, J. 2002, ApJ, 576, 222
Beckwith, S. V. W., & Sargent, A. I. 1991, ApJ, 381, 250
Beckwith, S. V. W., & Sargent, A. I. 1993, ApJ, 402, 280
Blandford, R. D., & Payne, D. G. 1982, MNRAS, 199, 883
Cabrit, S. 2009, in Protostellar Jets in Context, Astrophys. Space Sci. Proc., eds. K. Tsinganos, T. Ray, & M. Stute, 247
Cabrit, S., Pety, J., Pesenti, N., & Dougados, C. 2006, A&A, 452, 897
Cerqueira, A. H., Velázquez, P. F., Raga, A. C., Vasconcelos, M. J., & de Colle, F. 2006, A&A, 448, 231

[3] See also Webpage Siess.

Coffey, D., Bacciotti, F., Woitas, J., Ray, T. P., & Eislöffel, J. 2004, ApJ, 604, 758
Coffey, D., Bacciotti, F., Ray, T. P., Eislöffel, J., & Woitas, J. 2007, ApJ, 663, 350
Coffey, D., Rigliaco, E., Bacciotti, F., Ray, T. P., & Eislöffel, J. 2012, ApJ, 749, 139
Coffey, D., Dougados, C., Cabrit, S., Pety, J., & Bacciotti, F. 2015, ApJ, 804, 2
Comerón, F., & Fernández, M. 2010, A&A, 511, A10
Dartois, E., Dutrey, A., & Guilloteau, S. 2003, A&A, 399, 773
Duvert, G., Guilloteau, S., Ménard, F., Simon, M., & Dutrey, A. 2000, A&A, 355, 165
Fendt, C., Vaidya, B., Porth, O., & Nezami, S. S. 2011, in IAU Symp. 275, eds. G. E. Romero, R. A. Sunyaev, & T. Belloni, 383
Ferreira, J., Dougados, C., & Cabrit, S. 2006, A&A, 453, 785
Galli, P. A. B., Bertout, C., Teixeira, R., & Ducourant, C. 2013, A&A, 558, A77
Graham, J. A., & Heyer, M. H. 1988, PASP, 100, 1529
Guilloteau, S., & Dutrey, A. 1994, A&A, 291, L23
Hildebrand, R. H. 1983, QJRAS, 24, 267
Hughes, J., Hartigan, P., Krautter, J., & Kelemen, J. 1994, AJ, 108, 1071
Isella, A., Carpenter, J. M., & Sargent, A. I. 2009, ApJ, 701, 260
James, D. J., Melo, C., Santos, N. C., & Bouvier, J. 2006, A&A, 446, 971
Krautter, J. 1986, A&A, 161, 195
McMullin, J. P., Shiebel, D. R., Young, W., & Debonis, D. 2006, in Astronomical Data Analysis Software and Systems XV, eds. C. Gabriel, C. Arviset, D. Ponz, & S. Enrique, ASP Conf. Ser., 351, 319
Merín, B., Jørgensen, J., Spezzi, L., et al. 2008, ApJS, 177, 551
Mortier, A., Oliveira, I., & van Dishoeck, E. F. 2011, MNRAS, 418, 1194
Petrov, P. P., Gahm, G. F., Gameiro, J. F., et al. 2001, A&A, 369, 993
Pudritz, R. E., Ouyed, R., Fendt, C., & Brandenburg, A. 2007, Protostars and Planets V, 277
Ray, T., Dougados, C., Bacciotti, F., Eislöffel, J., & Chrysostomou, A. 2007, Protostars and Planets V, 231
Romanova, M. M., Ustyugova, G. V., Koldoba, A. V., & Lovelace, R. V. E. 2009, MNRAS, 399, 1802
Sauty, C., Cayatte, V., Lima, J. J. G., Matsakos, T., & Tsinganos, K. 2012, ApJ, 759, L1
Schwartz, R. D. 1977, ApJS, 35, 161
Shang, H., Li, Z.-Y., & Hirano, N. 2007, Protostars and Planets V, 261
Siess, L., Dufour, E., & Forestini, M. 2000, A&A, 358, 593
Staff, J. E., Koning, N., Ouyed, R., Thompson, A., & Pudritz, R. E. 2015, MNRAS, 446, 3975
Testi, L., Bacciotti, F., Sargent, A. I., Ray, T. P., & Eislöffel, J. 2002, A&A, 394, L31
The, P.-S. 1962, Contributions from the Bosscha Observervatory, 15
Wang, H., & Henning, T. 2009, AJ, 138, 1072
White, M. C., Bicknell, G. V., McGregor, P. J., & Salmeron, R. 2014, MNRAS, 442, 28
Woitas, J., Bacciotti, F., Ray, T. P., et al. 2005, A&A, 432, 149

Appendix A: Jet inclination

We revisit here previous estimates of the jet inclination to the line of sight. We use our adopted distance of $d = 185$ pc and consistent line-of-sight and plane-of-sky velocities for the distant knots. We assumed these knots to be terminal bow shocks, in which the pattern of peaks luminosity move together with the matter within.

Along the PA of 98°, a few HH knots were identified, especially one on the east side and one on the west side of the central source, designated as HH 228 E1, and W (Krautter 1986; Graham & Heyer 1988). Line-of-sight velocities ($V_{\rm rad}$) of -62 km s^{-1} and $+38$ km s^{-1} were reported for the E1 and W knots, respectively (Comerón & Fernández 2010). The Th 28 jet was observed at different epochs, which allowed Wang & Henning (2009) to derive proper motions for the knots mentioned above. They found a proper motion of 0.47″ yr^{-1} for the E1 knot, and 0.37″ yr^{-1} for the W knot.

At the adopted distance for Th 28 of $185\pm^{11}_{10}$ pc, it corresponds to proper motions of 412 ± 25 km s^{-1} and 324 ± 20 km s^{-1} for the E1 and W knots, respectively. This provides independent measurements of the inclination of the system via inclination $= \arctan\left(\dfrac{V_{\rm rad}}{\text{proper motion}}\right)$, of $81.3 \pm 1°$ and $83.2 \pm 1°$ for the E1 and W knots, respectively. We therefore adopt a global inclination of the jet, from the knots analysis, of $82.3 \pm 2°$.